Adsorption (2012) 18:483–491
DOI 10.1007/s10450-012-9438-7

Synthesis, characterization, and hydrogen storage study by hydrogen spillover of MIL-101 metal organic frameworks

Kuen-Song Lin · Abhijit Krishna Adhikari · Yu-Hsien Su · Chia-Wei Shu · Ho-Yang Chan

Received: 23 May 2012 / Accepted: 4 October 2012 / Published online: 12 October 2012

Abstract MIL-101 is a chromium-based metal organic framework known to adsorb large amount of gases such as H_2, CO_2 and CH_4. The framework was synthesized through solvothermal route and the H_2 adsorption capacity was measured using a standard gravimetric method. X-ray absorption spectroscopy was performed to understand the fine structure, neighbors, coordination number and bond distance. The BET specific surface area of MIL-101nf (treated with NH_4F) was 2,868 m^2/g with a type I hysteresis loop measured from N_2 adsorption isotherm. The hydrogen storage capacity was 0.16 wt% measured at 32 bar and room temperature for MIL-101nf. This capacity was increased up to 0.45 wt% by doping metal-supported carbon catalyst (Pd/AC and Pt/AC) through a carbon bridge with MIL-101. XANES spectra indicated that the valency of MIL-101 MOFs was Cr(III). EXAFS data also revealed that MIL-101 has a first shell of Cr-O bonding with the bond distance of 1.97 Å and the coordination number of 5.4.

Keywords MIL-101 · Metal organic frameworks · Porous material · Hydrogen storage · XANES/EXAFS · Hydrogen spillover

1 Introduction

The negative impact of greenhouse gases and the eventual depletion of fossil fuel reserves have increased the importance of developing alternative fuel sources that are strong, viable, and emission free. Hydrogen is considered as a clean fuel that has a minimum impact on the environment nearly eliminating the levels of carbon dioxide and other greenhouse gas emissions (Mazloomi and Gomes 2012). It is safe to manufacture, reliable and environmental friendly (Nowotny et al. 2005; Uhm et al. 2012). Also, demanding for more efficient power source has increased the interest in different kinds of new technologies, such as fuel cells using hydrogen or hydrocarbons as fuel (Avc et al. 2001; Martin et al. 2009; Suzuki et al. 2011). It is widely believed that hydrogen will become the fuel of the near future that powers most vehicles and portable devices. Hydrogen will become the means of storing and transporting energy. However, developing safe, reliable, compact, and cost-effective H_2 storage technologies is one of the most technically challenging barriers to the widespread use of hydrogen as a form of energy as well as onboard vehicle application. Hydrogen storage by adsorption represents a potential strategy for effective and relatively safe hydrogen storage. Many efforts have been expended to finding efficient hydrogen storage materials. Concerning adsorbents, nanostructured carbon including activated carbon (AC) (Erdogan and Kopac 2007), carbon nanotubes (Hirscher and Becher 2003) graphite nanofibers (Lueking et al. 2004), zeolites (Dong et al. 2007) and complex metal hydrides (Sakintuna et al. 2007) have been the major candidates for hydrogen storage. However, known carbon nanostructures and other studied materials cannot store a sufficient amount of H_2 required for transportation applications (Luo and Rönnebro 2005; Armaroli and Balzani 2011).

Metal-organic frameworks (MOFs) are a rapidly growing class of microporous materials that enable tailoring of regular porosity on a nanometer scale (Rowsell et al. 2005). A variety of MOFs have been studied past few years for many potential applications, such as optics(Evans and Lin 2002), adsorptions depending on size and shape (Saha

K.-S. Lin (✉) · A.K. Adhikari · Y.-H. Su · C.-W. Shu · H.-Y. Chan
Department of Chemical Engineering and Materials Science/Fuel Cell Center, Yuan Ze University, Chung-Li City 32003, Taiwan
e-mail: kslin@saturn.yzu.edu.tw

and Deng 2010), catalysis (Bandosz and Petit 2011), and most importantly gas storage (Rowsell and Yaghi 2004; Lin et al. 2011). Among the potential applications, particularly, MOFs have been explored as a viable H_2 storage material due to their relatively high hydrogen storage capacity and raised considerable interest in this field (Panella et al. 2006; Saha et al. 2008). MOFs have the advantages of reversibility and fast kinetic ability in H_2 adsorption than complex metal hydrides. However, it is still far away from the hydrogen adsorption goal for onboard vehicle established by the United States Department of Energy (DOE). Recently, hydrogen spillover effect was successfully used in hydrogen storage materials based on physisorption, such as carbon materials (Wang and Yang 2012), zeolites (Li and Yang 2006a), MOFs (Stuckert et al. 2010; Wang et al. 2011). Hydrogen storage capacity of porous materials can be greatly enhanced by doping them with metal supported catalysts through a carbon bridge. The increased hydrogen storage capacity of catalyst-doped porous materials is attributed to the hydrogen spillover effect. The process includes a dissociation of hydrogen molecules on a metal and subsequent spillover to its support, while the carbon bridge helps the hydrogen to spillover to the target porous materials that formed the secondary spillover. This process modifies the chemical nature of the porous materials and activates the porous materials to strengthen subsequent hydrogen physisorption (Roland et al. 1997).

In this view, we tried to focus the hydrogen spillover effect on MIL-101 metal organic framework. A past study showed that it could store 0.36 wt% of hydrogen at 298 K and 86 bar (Latroche et al. 2006). Here we present our results on hydrogen storage capacity of MIL-101 doped with Pt/AC or Pd/AC catalyst and modified with carbon bridged Pt/AC or Pd/AC. We also focused on the fine structural characterization of MIL-101 with short-range order through X-ray absorption spectroscopy (XAS) such as; X-Ray absorption near edge spectroscopy (XANES) which provides information of electronic configuration, stereochemistry and the oxidation states of the metallic atoms in the catalysts and extended X-ray absorption fine structure (EXAFS) spectroscopy which can investigate the information on the atomic arrangement of the catalysts in terms of bond distance, coordination number, kind of neighbors, thermal and static disorder (Meitzner et al. 1992; Zabinsky et al. 1995). The XANES and EXAFS also offer the basic knowledge of understanding the oxidation states and fine structures to further study on the mechanism of surface reaction. Thus, the main objectives of the present work were to investigate the effects of different activation process of MIL-101, carried out the valency and fine structural parameters of Cr atom in MIL-101 as central metal ion and the hydrogen storage capacity via hydrogen spillover.

2 Experimental

2.1 Synthesis of MIL-101 samples

MIL-101 was synthesized through solvothermal route that can be found in literature (Fèrey et al. 2005). 2.0 g Chromium nitrate nano hydrate ($Cr(NO_3)_3{\cdot}9H_2O$) and 0.83 g of BDC (Terephthalic acid) were dissolved in 24 mL of deionized water following the addition of 0.9 mL hydrofluorohydric acid (HF, 5 M). After stirring the above mixture about 15 min, it was introduced into Teflon-lined steel autoclave to heat at 220 °C for 8 h. Then the autoclave was cooled slowly in room temperature. The nonreacted BDC was present in the green color crystals and it was removed by filtering through glass frit. Then the product was washed with deionized water several times and dried. This product is denoted as MIL-101as (as: as-synthesized). Then about 2.0 g of MIL-101as sample was treated with 40 mL aqueous mixture of ethanol (95 % ethanol and 5 % water) at 60 °C for 20 h. After cooling the sample was washed and dried at 100 °C overnight. At this stage it is denoted as MIL-101et (et: ethanol treated). Finally, 2.0 g of MIL-101et sample was treated with 300 mL NH_4F (30 mM) at 60 °C for 12 h. Then the sample was washing several times, drying at 100 °C and denoted as MIL-101nf (nf: NH_4F treated). These all treatments were done due to purify the crystals as purification and activation of MIL-101 are very crucial.

2.2 Preparation of Pt or Pd-doped AC (Pt/AC and Pd/AC)

In a typical procedure to synthesize the Pt or Pd-doped AC, Darco AC of 100-325 mesh obtained from Sigma-Aldrich was further treated by nitric acid in this work. 5.0 g of AC was immerged into 300 mL of 3M nitric acid solution. The resulting mixture was heated to 60 °C and stirred for 1 h. After cooling to room temperature the AC was filtered and washed with water until the pH 5 had been reached and then dried in air. 0.5 g $PtCl_4$ or $PdCl_4{\cdot}5H_2O$ was dissolved into another 300 mL of H_2O/ethylene glycol solution with the volume ratio of 1:2. Then the acid treated AC was added into the H_2O/ethylene glycol solution and stirred for 12 h at 110 °C. Then the resulted mixture was filtered and the solid residue was dried at 70 °C overnight in reduced pressure. The Pt or Pd content into AC was found around 5 wt% analyzed by ICP-OES.

2.3 Preparation of Pt or Pd-doped AC–MIL-101

An effective bridged composite of Pt or Pd-doped AC–MOFs was done by building technique (Lachawiec et al. 2005; Li and Yang 2006b). The catalyst containing 5 wt% platinum or palladium supported on active carbon was used as the source for hydrogen dissociation. Carbon bridges

between the source and receptor were formed by carbonization of sucrose that was previously introduced into a physical mixture with Pt/AC or Pd/AC. The receptor/precursor/source ratio was fixed at 4:1:1 on the basis of the complete carbonization of the precursor. The resultant mixture was ground together for 1 h in ball mill and then subjected to the heating treatment procedures as described by Li and Yang (2006b).

2.4 Characterization

X-ray diffraction (XRD) measurements were conducted using standard powder diffraction procedures analyzed by Cu Kα radiation (RIGAKU Model D/MAX III-V) at 30 kV and 20 mA with a scan rate of $4°(2\theta)$ min^{-1}. FE-SEM (S-4700 Type II) and TEM (Zeiss 10C) were performed to identify the morphologies, and particle size distribution of the crystals. ICP-OES was performed by Optima 2100DV (Perkin Elmer) for item analyses of the samples. Nitrogen adsorption isotherms of the samples were measured at 77 K using an ASAP 2020 (Micromeritics). Thermal decomposition was investigated using a TGA system (model SDT 2960 & Thermal Analyst 2000, TA Instruments). Reaction temperatures and sample weights were recorded at 10 seconds intervals. About 30 mg of samples were heated from 25 to 600 °C at a heating rate of 10 °C min^{-1} in air atmosphere at the flow rate of 20 cm^3 min^{-1}.

X-ray absorption (EXAFS and XANES) spectra were collected at the Wiggler beam line 16A1 at NSRRC of Taiwan. The electron storage ring was operated with an energy of 1.5 GeV and the current of 100–200 mA. A Si (111) double-crystal monochromator (DCM) was used for selection of energy with an energy resolution of 1.9×10^{-4}. Data were collected in fluorescence or transmission mode with a Lytle detector (Lytle 1999) in the regions of the Cr K edge (5,989 eV) at room temperature. The photon energy was calibrated by characteristic pre-edge peaks in the absorption spectra of Cr standards. The raw absorption data below the edge position were fit to a straight line using the least-square algorithms. The fitted pre-edge background curves were extrapolated throughout all data range, subtracted and normalized to minimize the effect of sample thickness. The near-edge structure in an absorption spectrum covers the range between the threshold and the point at which the EXAFS begins. The k^2 and k^3-weighted EXAFS spectra were Fourier transformed over the range of interatomic distance (R). The EXAFS data were further analyzed by using the UWXAFS 3.0 program and FEFF 8.0 codes (Ressler 1998; Nesvizhskii and Rehr 1999).

2.5 Hydrogen adsorption measurement

Hydrogen isotherm was measured gravimetrically at 298 K using a method previously described by Eddaoudi et al. (2000). A Cahn Thermax 500 microgravimetric balance was used to measure the change in mass of samples suspended within a glass enclosure under a certain atmosphere which had a sensitivity of 1 µg. A pressure sensor, with a range of 0 to 68 atm (at 1,000 °C) and sensitivity of 0.011 atm was used to measure the hydrogen pressure in the chamber. Samples were outgassed overnight in situ until constant mass was attained; these varied from 0.2 to 2.0 g. Prior to admittance of the analyte gas, the entire chamber and manifold were evacuated overnight. The system was purged at room temperature three times with the analyte gas before cooling to 77 K, and gases were passed through a molecular sieve trap immersed in liquid nitrogen to remove any condensable impurities or moisture before being exposed to the sample. The adsorbed amount of hydrogen gas was calculated after the buoyancy correction of the experiment. For the buoyancy correction, the volume of the sample container and the sample was determined using a helium measurement assuming that helium adsorption at room temperature can be neglected.

3 Results and discussion

3.1 Morphologies of MIL-101 samples

FE-SEM and TEM micrographs of MIL-101 and Pt or Pd-doped AC were used to investigate the morphologies, and microstructure of the samples. The particle size of synthesized MIL-101 samples was around 500–700 nm identified by FE-SEM micrographs shown in Fig. 1a. It has an octahedral shape and the particles are well dispersed. TEM images of Pd/AC and Pt/AC are shown in Figs. 1b and 1c, respectively. Pt and Pd particles were uniformly dispersed in AC and the particle size was very small which is favorable to enhance the spillover. The particle size of Pd for 5 wt% Pd/AC ranges from 5 to 15 nm while the Pd particles were much smaller around 2 to 10 nm. Formation of large Pt or Pd particles can be attributed to the aggregation of some smaller particles. All the particles were well dispersed in AC that facilitated the spillover of hydrogen by dissociating of hydrogen molecule into atomic hydrogen.

3.2 Crystallinity analysis

The XRD patterns of three different MIL-101 samples (MIL-101as, MIL-101et and MIL-101nf) are plotted in Fig. 2. All samples showed good crystallinity though there were notable changes had been found on the intensity of the peaks. It can be found that the peak intensities around 17.40 2θ degree of MIL-101as showed higher values than MIL-101et and MIL-101nf samples. There may remain some small amount of unreacted chemicals that has been removed

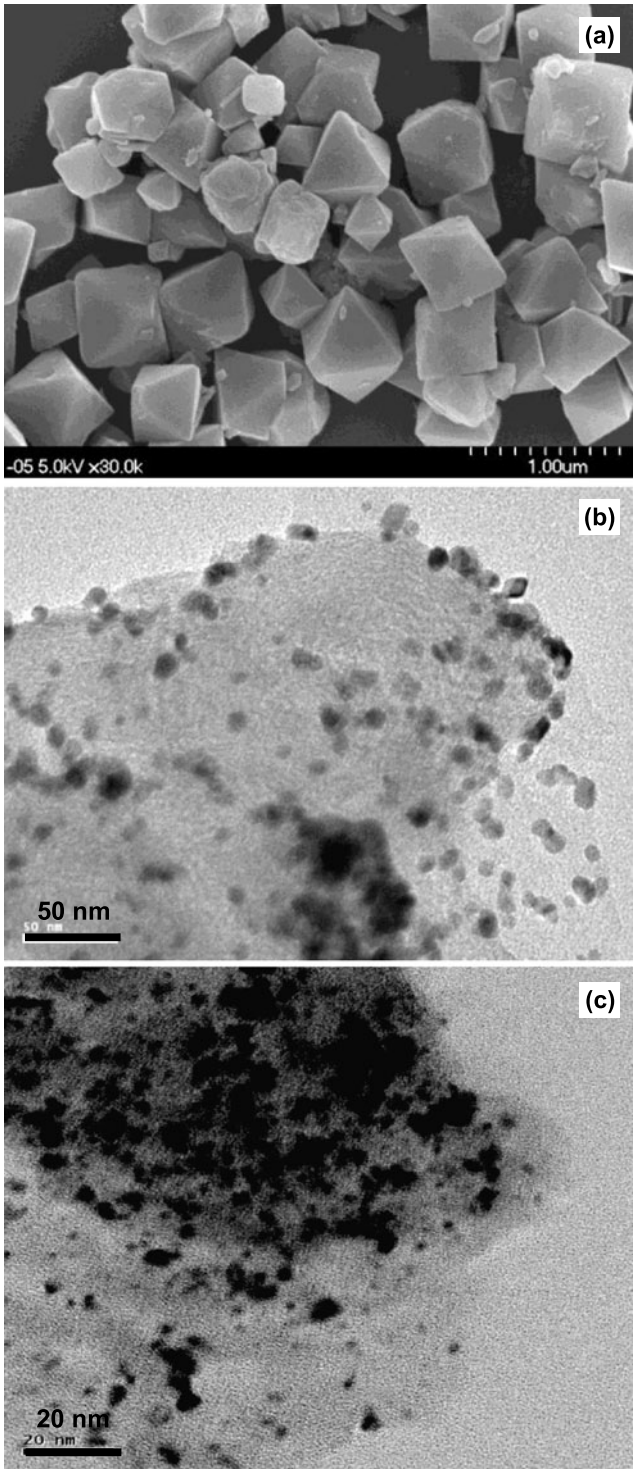

Fig. 1 (**a**) FE-SEM images of MIL-101 after treated by using NH_4F; TEM images of (**b**) Pd-doped AC, and (**c**) Pt-doped AC

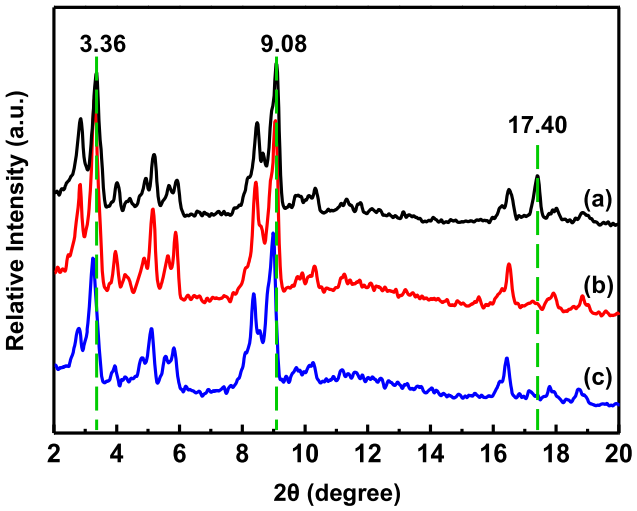

Fig. 2 XRD patterns of MIL-101 for (**a**) as-synthesized, treated by (**b**) ethanol, and (**c**) NH_4F

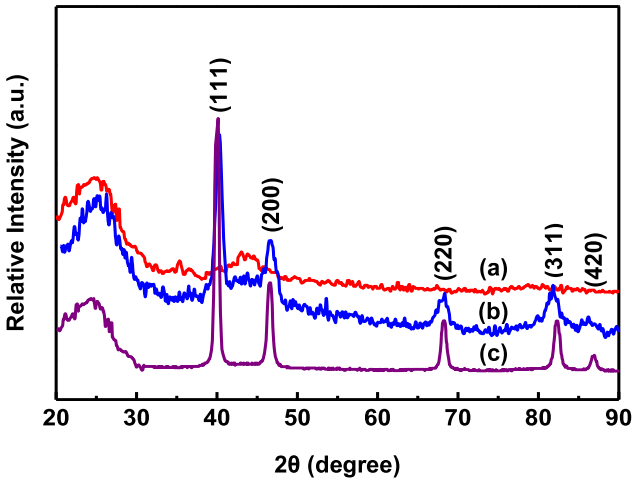

Fig. 3 XRD patterns of (**a**) activated carbon, (**b**) Pd-doped AC, and (**c**) Pt-doped AC

after ethanol treatment. The intensive peaks appearing at small 2θ angles in the XRD pattern are characteristics of porous materials which possess abundant pores or cavities. The main diffraction peaks were at $2\theta = 3.36$, 5.10, 8.41, 9.08, and 16.46 degree. The relative diffraction intensities of the prepared samples were found to be the same as the standard data for MIL-101 (Fèrey et al. 2005). Figure 3 shows the XRD patterns of AC, Pd-doped AC, and Pt-doped AC. These patterns show a broad and less intensive peak around $2\theta = 24$ degree can be attributed to the graphitic structure of AC. The other four peaks could be indexed to the (111), (200), (220), and (311) planes of Pd or Pt catalysts (Liu et al. 2007b). The calculated mean particle size of the doped Pd and Pt particles by Scherrer equation were about 18 and 14 nm, respectively.

3.3 Thermal analysis

As shown in Fig. 4, the thermogravimetric curve of MIL-101 MOF is consistent with prominent weight-loss steps. It followed that a fully hydrated molecular sieve contains about

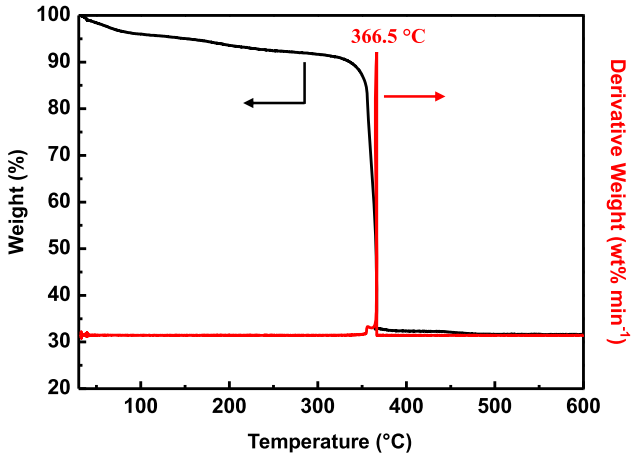

Fig. 4 TG/DTG curve of as-synthesized MIL-101

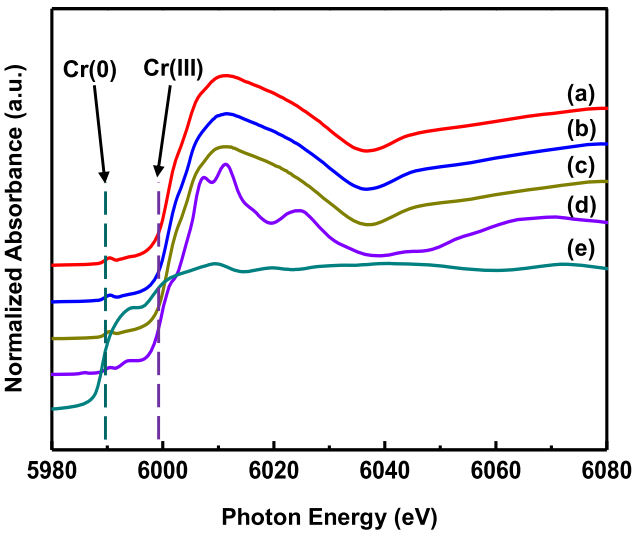

Fig. 5 Normalized Cr K-edge XANES spectra of MIL-101 for (**a**) as-synthesized, (**b**) treated by ethanol, (**c**) treated by NH_4F, (**d**) Cr_2O_3, and (**e**) Cr(0) standards

8 wt% water and other guest molecules. At the initial period (25–200 °C) the weight loss is due to the evaporation of water or guest molecules. It has also to be mentioned that the water content of MIL-101 varies considerably, depending on the presence of coordinated solvent, the temperature in the laboratory, or the rate of humidity. After that the sample didn't show any step of weight change but slow and gradually decay in weight until 340 °C. This result confirmed the stability of the framework at higher temperature and a sudden weight change (around 56 wt%) was observed around 366 °C due to the total damage of organic linker.

3.4 XANES measurement

The normalized Cr K-edge XANES of three different MIL-101 samples with the Cr_2O_3, and Cr(0) standards are represented in Fig. 5. The comparison is designed to determine the Cr atoms in MIL-101 MOFs and understanding the treatment effects of ethanol and NH_4F on the crystal structures. It was found that the edge positions of all the prepared samples were very close to the Cr(II) as shown in Table 1. However, compared with the standard Cr(II) K-edge energy (5,989 eV) the offset was 0.16 eV for the MIL-101as sample which revealed that Cr ions were not entirely surrounded by oxygen atoms and may form oxides (OH^-) through covalent bond. The offset of MIL-101et and MIL-101nf samples were around 0.12 eV which can also speculated for Cr(II) ions during the elimination of the nonreacted BDC molecules upon treatment with ethanol and NH_4F. The pre-edge XANES spectra of Cr exhibit an absorbance feature at 5,991 eV for the $1s$ to $3d$ transition and this transition is forbidden by the selection rule in case of perfect octahedral symmetry. The sharp feature at 6,010 eV of MIL-101as, due to the dipole-allowed $1s$ to $4p_{xy}$ electron transition, indicated the existence of Cr^{2+}. The density of Cr^{2+} in MIL-101 was proportional to the intensity of the $1s$ to $4p_{xy}$ transition. The shoulder at 6,001 eV and an intense feature at 6,011 eV for MIL-101et and MIL-10nf samples were attributed to the $1s$ to $4p_{xy}$ transition also, that indicated the existence of Cr^{2+} species in the MIL-101 crystals. Oxygen is the major atoms coordinated to the central Cr atoms in the prepared crystals.

Table 1 Chromium K-edge X-ray absorption near-edge position of MIL-101 samples

Sample	Shell	Near edge (eV)
MIL-101 as-synthesized	Cr–O	6001.10
MIL-101 treated by ethanol	Cr–O	6000.62
MIL-101treated by NH_4F	Cr–O	6000.88
Cr_2O_3	Cr–O	6005.85
Metallic Cr	Cr–Cr	5988.90

3.5 EXAFS analysis

The MIL-101 samples were further studied by using EXAFS to understand the fine structure and the behavior in the neighbor atoms. Cr K-edge EXAFS spectroscopy can also provide the information on the Cr atomic arrangement of catalysts in terms of bond distance, coordination number, and kind of near neighbors. Figure 6 shows the k^3-weighted and least-square fitted Cr K-edge EXAFS and their Fourier transforms of three different MIL-101 samples. Since XANES shows significant changes between as synthesized and treated MIL-101 samples, it is interesting that the EXAFS data shown in Table 2 are virtually identical. It shows that the all samples have the center Cr atoms coordinated by primarily Cr–O bonding. The fine structural parameters of MIL-101 analyzed by the EXAFS data also

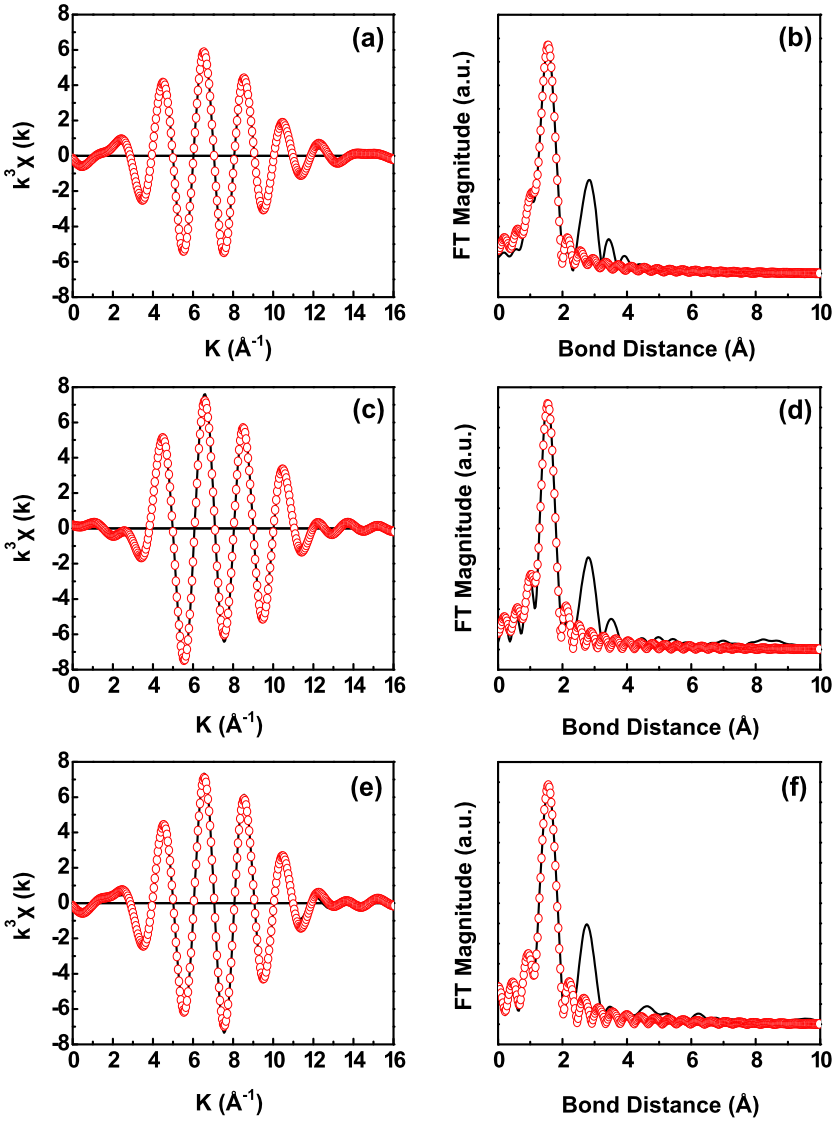

Fig. 6 Cr K-edge EXAFS oscillation $k^3\ \chi(k)$ and Fourier transform (FT) spectra of MIL-101 samples: (**a**), (**b**) as-synthesized, treated by (**c**), (**d**) ethanol, and (**e**), (**f**) NH_4F. The best fitting of the EXAFS spectra are expressed by the circled symbols

Table 2 Fine structural parameters of MIL-101 samples analyzed by using Cr K-edge EXAFS

Sample	Shell	CN[a] ± 0.5	R[b] ± 0.02 (Å)	$\Delta\sigma^2$[c] (Å^2)
MIL-101 as-synthesized	Cr–O	5.42	1.971	0.00582
MIL-101 treated by ethanol	Cr–O	4.74	1.973	0.00237
MIL-101treated by NH_4F	Cr–O	4.53	1.973	0.00302

[a]Coordination number

[b]Bond distance

[c]Debye-Waller factor

suggested that Cr atoms may be mirror-symmetrically (D_d) surrounded by four oxygen atoms. The EXAFS data showed that the MIL-101as sample had Cr central atoms coordinated by primarily Cr–O with the bond distances of 1.971 Å with the coordination number of 5.42. After the treatment with ethanol, the bond distance of Cr–O in MIL-101et was 1.973 Å with the coordination number of 4.73. Following the same trend, MIL-101nf had the less coordination number as 4.53 while it can be noted that, the bond distance didn't change compare to MIL-101et which is 1.973 Å. This is a statistical effect; this means that in spite of removing a small amount of oxygen atoms from the lattice, the overall

Table 3 The pore structural properties of MIL-101 samples, AC, Pd/AC, and Pt/AC

Sample	Activation method	BET surface area ($m^2\ g^{-1}$)	Pore volume ($cm^3\ g^{-1}$)[a]	Average pore size (Å)[a]
MIL-101 as-synthesized	N.A.[b]	1452	0.016	8.03
MIL-101 treated by ethanol	Ethanol	2454	0.020	8.04
MIL-101treated by NH_4F	NH_4F	2868	0.025	8.06
AC after acid treatment	HNO_3, 3M	840	0.062	8.04
Pd/AC	N.A.[b]	655	0.061	8.04
Pt/AC	N.A.[b]	619	0.055	8.03

[a]Pore volume and average pore size were determined by DFT method

[b]N.A. denotes "not available"

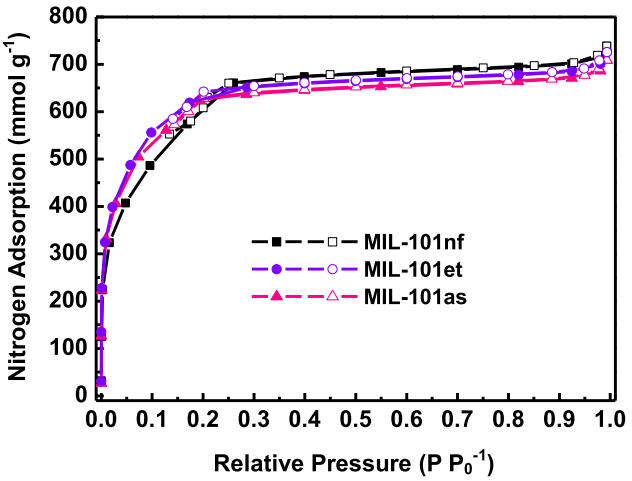

Fig. 7 BET nitrogen adsorption isotherms of as-synthesized, ethanol and NH_4F treated MIL-101 samples measured at 77 K. Filled and open symbols represent the adsorption and desorption of nitrogen gases, respectively

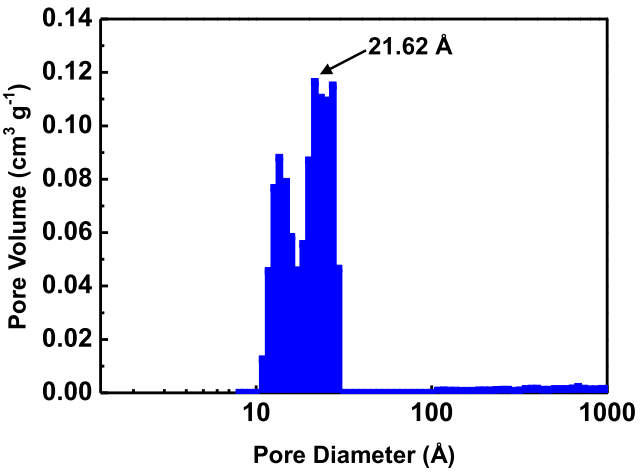

Fig. 8 Pore size distribution of as-synthesized MIL-101 measured by Density Functional Theory method

structure is maintained with little electronic changes. These oxygen atoms may contributed from the non-reacted BDC that presents in the MIL-101as structure. As MIL-101et and MIL-nf samples are treated, the number of non-reacted BDC present in the structure are very few, hence the coordination number decreased.

3.6 Pore textural properties

Table 3 summarizes the pore textural properties for the three samples of MIL-101 along with AC and Pt or Pd-doped AC. The nitrogen adsorption isotherms of different MIL-101 samples measured at 77 K are shown in Fig. 7. Both isotherms were type-I with almost no hysteresis loop. It confirms that the MIL-101 samples were microporous. The BET specific surface area was measured using Barret–Joyner–Halenda (BJH) model (Barrett et al. 1951), while pore volume and average pore diameter were calculated by the ASAP 2020 analyzer's built-in software using Density Functional Theory (DFT) method. It was noted that the BET specific surface area notably increases with after treated the MIL-101as sample with ethanol and NH_4F. For the as synthesized MIL-101 the BET specific surface area was 1,452 $m^2\ g^{-1}$. After ethanol treatment this value enhanced to 2,454 $m^2\ g^{-1}$ for MIL-101et and from this situation, finally it increased to 2,868 $m^2\ g^{-1}$ for MIL-101nf. These results proves that post treatment is crucial for MIL-101 samples to improve the surface area which is favorable for the higher hydrogen storage (Llewellyn et al. 2008). The pore textural properties of the three MIL-101 samples had the similar trend to increase the pore volume with the treatment with ethanol and NH_4F. The discrepancies between the observed values are due to the variable amount of terephthalic acid present as an impurity or present within the pores. The presence of free terephthalic acid within the pores of MIL-101 was expected since other porous chromium (Barthelet et al. 2004) terephthalates contained significant amounts of free carboxylic acid within the pores in their as-synthesized form. The BET specific area of AC after acid treatment was 840 $m^2\ g^{-1}$. After Pt or Pd-doping, this value was decreased to 619 or 655 $m^2\ g^{-1}$, respectively. The pore size distribution of MIL-101as sample is shown in Fig. 8. It can be seen that the average pore size of the synthesized sample was about 21.62 Å with the pore volumes vary between 0.016 and 0.025 $cm^3\ g^{-1}$.

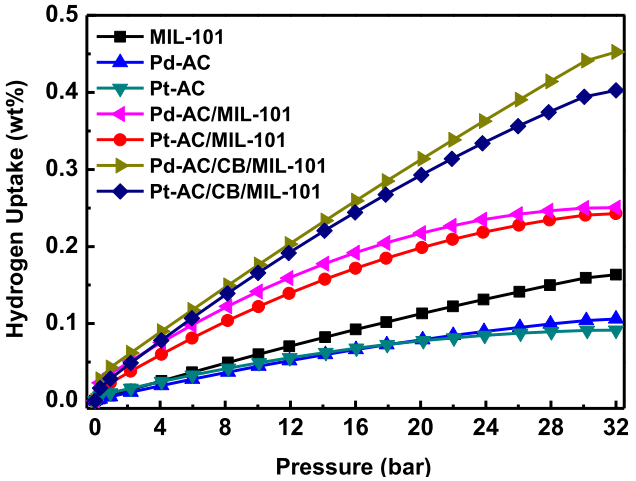

Fig. 9 Hydrogen adsorption isotherms of Pt-doped AC, Pd-doped AC and different MIL-101 samples measured at $T = 298$ K and $P = 0$–32 bar

3.7 Gravimetric hydrogen adsorption

The hydrogen adsorption isotherms of the MIL-101 materials measured at room temperature (298 K) are presented in Fig. 9. We have used the NH_4F treated MIL-101 sample to examine the hydrogen adsorption capacity as it has the highest BET specific surface area. It can be seen that the H_2 adsorption value of MIL-101 sample without Pt or Pd-doped was about 0.16 wt%. The H_2 adsorption capacity for Pd-AC and Pt-AC were about 0.11 and 0.09 wt%, respectively. It can be noted that Pd-AC and Pt-AC have lower H_2 adsorption capacity than pristine MIL-101 sample though they have primary spillover effect. It may be due to the lower specific surface area of Pd-AC or Pt-AC samples. After mixing the Pd-AC or Pt-AC with MIL-101 sample, the H_2 adsorption capacity increased to 0.25 and 0.24 wt%, respectively. This elevated adsorption capacity of MIL-101 sample was due to the additional H_2 adsorption by the Pd-AC or Pt-AC. However, after establishing the carbon bridge between MIL-101 and Pd-AC or Pt-AC, the H_2 adsorption capacity increased to 0.45 and 0.40 wt% through hydrogen spillover mechanism. The enhancement factor is defined as the ratio of the adsorbed amount of the bridged sample via spillover to that of the MIL-101 alone. After the modification of MIL-101, this factor is almost three times that of the unmodified MIL-101. There are two reasons for this significant improvement: the first reason is the role of AC as a support for Pd or Pt catalytic activity. The Pd or Pt nanoparticles are uniformly distributed into the AC supports. Therefore, the dissociation of hydrogen molecule is improved through the catalytic activity of Pd or Pt which has led to significant changes in hydrogen sorption properties. This is the primary spillover effect. The second reason is the carbon bridge and making of site defect in carbon supported sample. The bridge-building treatment strengthens the connectivity between MIL-101 and Pd/AC or Pt/AC, and the migration of monatomic hydrogen, largely enhancing hydrogen uptake. After the bridge-building treatment, Pd/AC or Pt/AC particles (primary spillover receptor) were well dispersed within fine powders of MIL-101 crystals (secondary spillover receptor) through the connection of carbon bridges. Generally, at the low-pressure region of the adsorption isotherm, it is strongly dependent on the strength of the interaction between hydrogen molecules and the adsorbent. Therefore, the difference in the storage capacity and different heat of adsorption are attributed. The presence of amorphous or nonporous impurity such as the impurities during the synthesis process is also required to eliminate for enhancing the hydrogen uptake (Lee et al. 2005; Rowsell and Yaghi 2006; Liu et al. 2007a). Activation involves removal of any guest molecules (most of them are synthesis solvent and the excess organic ligands) that are contained within the pores or channels of the MIL-101 MOFs, either through thermal or chemical means or through a combination of both. In the case of H_2 adsorption measurements, there are additional considerations should taken such as the experimental system must be ultra-clean and it is necessary to purify even ultrahigh-purity hydrogen before the measurements.

4 Conclusions

MIL-101 MOFs having the particle size about 500–700 nm and crystalline in structure. The central Cr atom of as synthesized MIL-101 was coordinated by primarily Cr–O bonds having the bond distance of 1.971 Å with the coordination number of 5.42. After treatment with ethanol and NH_4F, the Cr–O bonds distance changed into 1.973 Å with the coordination number of 4.53. The Cr atom was in divalent (Cr^{2+}) in the MIL-101 crystals identified by XANES spectra. The results show an improvement in the hydrogen adsorption capacity after modifying the MIL-101 with Pd-AC or Pt-AC and carbon bridge. The storage capacity of modified MIL-101 at 32 bar and 298 K are found to be 0.45 wt% (MIL-101/CB/Pd-AC) and 0.40 wt% (MIL-101/CB/Pt-AC) which is significantly improved as compared to the pristine sample (0.16 wt% at 298 K and 32 bar).

Acknowledgements The financial support of the National Science Council, Taiwan (NSC-94-2211-E-155-001) is gratefully acknowledged. We also thank Prof. Y.W. Yang and Dr. J.F. Lee of the Taiwan Synchrotron Radiation Research Center (NSRRC) for helping to perform XAS experiments.

References

Armaroli, N., Balzani, V.: The hydrogen issue. ChemSusChem **4**(1), 21–36 (2011)

Avc, A.K., Ilsenänsan, Z., Trimm, D.L.: On-board fuel conversion for hydrogen fuel cells: comparison of different fuels by computer simulations. Appl. Catal. A, Gen. **216**(1–2), 243–256 (2001)

Bandosz, T.J., Petit, C.: MOF/graphite oxide hybrid materials: exploring the new concept of adsorbents and catalysts. Adsorption **17**(1), 5–16 (2011)

Barrett, E.P., Joyner, L.G., Halenda, P.P.: The determination of pore volume and area distributions in porous substances. I. Computations from nitrogen isotherms. J. Am. Chem. Soc. **73**(1), 373–380 (1951)

Barthelet, K., Marrot, J., Ferey, G., Riou, D.: $V^{III}(OH)\{O_2C–C_6H_4–CO_2\}\cdot(HO_2C–C_6H_4–CO_2H)_x(DMF)_y(H_2O)_z$ (or MIL-68), a new vanadocarboxylate with a large pore hybrid topology: reticular synthesis with infinite inorganic building blocks? Chem. Commun. **5**, 520–521 (2004)

Dong, J., Wang, X., Xu, H., Zhao, Q., Li, J.: Hydrogen storage in several microporous zeolites. Int. J. Hydrog. Energy **32**(18), 4998–5004 (2007)

Eddaoudi, M., Li, H.L., Yaghi, O.M.: Highly porous and stable metal-organic frameworks: structure design and sorption properties. J. Am. Chem. Soc. **122**(7), 1391–1397 (2000)

Erdogan, F.O., Kopac, T.: Dynamic analysis of sorption of hydrogen in activated carbon. Int. J. Hydrog. Energy **32**(15), 3448–3456 (2007)

Evans, O.R., Lin, W.: Crystal engineering of NLO materials based on metal-organic coordination networks. Acc. Chem. Res. **35**(7), 511–522 (2002)

Fèrey, G., Mellot-Draznieks, C., Serre, C., Millange, F., Dutour, J., Surble, S., Margiolaki, I.: A chromium terephthalate-based solid with unusually large pore volumes and surface area. Science **309**(5743), 2040–2042 (2005)

Hirscher, M., Becher, M.: Hydrogen storage in carbon nanotubes. J. Nanosci. Nanotechnol. **3**(1–2), 3–17 (2003)

Lachawiec, A.J., Qi, G., Yang, R.T.: Hydrogen storage in nanostructured carbons by spillover: bridge-building enhancement. Langmuir **21**(24), 11418–11424 (2005)

Latroche, M., Surblé, S., Serre, C., Mellot-Draznieks, C., Llewellyn, P.L., Lee, J.-H., Chang, J.-S., Jhung, S.H., Férey, G.: Hydrogen storage in the giant-pore metal-organic frameworks MIL-100 and MIL-101. Angew. Chem. Int. Ed. **45**(48), 8227–8231 (2006)

Lee, J., Li, J., Jagiello, J.: Gas sorption properties of microporous metal organic frameworks. J. Solid State Chem. **178**(8), 2527–2532 (2005)

Li, Y., Yang, R.T.: Hydrogen storage in low silica type X zeolites. J. Phys. Chem. B **110**(34), 17175–17181 (2006a)

Li, Y., Yang, R.T.: Hydrogen storage in metal-organic frameworks by bridged hydrogen spillover. J. Am. Chem. Soc. **128**(25), 8136–8137 (2006b)

Lin, K.-S., Adhikari, A.K., Chang, K.-C., Tu, M.-T., Lu, W.: Hydrogen adsorption in metal organic frameworks by hydrogen spillover. Catal. Today **164**(1), 23–27 (2011)

Liu, J., Culp, J.T., Natesakhawat, S., Bockrath, B.C., Zande, B., Sankar, S.G., Garberoglio, G., Johnson, J.K.: Experimental and theoretical studies of gas adsorption in $Cu_3(BTC)_2$: an effective activation procedure. J. Phys. Chem. C **111**(26), 9305–9313 (2007a)

Liu, J.M., Meng, H., Li, J.L., Liao, S.J., Bu, J.H.: Preparation of high performance Pt/CNT catalysts stabilized by ethylenediaminetetraacetic acid disodium salt. Fuel Cells **7**(5), 402–407 (2007b)

Llewellyn, P.L., Bourrelly, S., Serre, C., Vimont, A., Daturi, M., Hamon, L., De Weireld, G., Chang, J.S., Hong, D.Y., Hwang, Y.K., Jhung, S.H., Fèrey, G.: High uptakes of CO_2 and CH_4 in mesoporous metal-organic frameworks MIL-100 and MIL-101. Langmuir **24**(14), 7245–7250 (2008)

Lueking, A.D., Yang, R.T., Rodriguez, N.M., Baker, R.T.K.: Hydrogen storage in graphite nanofibers: effect of synthesis catalyst and pretreatment conditions. Langmuir **20**(3), 714–721 (2004)

Luo, W., Rönnebro, E.: Towards a viable hydrogen storage system for transportation application. J. Alloys Compd. **404–406**, 392–395 (2005)

Lytle, F.W.: The EXAFS family tree: a personal history of the development of extended X-ray absorption fine structure. J. Synchrotron Radiat. **6**, 123–134 (1999)

Martin, E., Shaheen, S.A., Lipman, T.E., Lidicker, J.R.: Behavioral response to hydrogen fuel cell vehicles and refueling: results of California drive clinics. Int. J. Hydrog. Energy **34**(20), 8670–8680 (2009)

Mazloomi, K., Gomes, C.: Hydrogen as an energy carrier: prospects and challenges. Renew. Sustain. Energy Rev. **16**(5), 3024–3033 (2012)

Meitzner, G., Via, G.H., Lytle, F.W., Sinfelt, J.H.: Analysis of X-ray absorption edge data on metal catalysts. J. Phys. Chem. **96**(12), 4960–4964 (1992)

Nesvizhskii, A.I., Rehr, J.J.: L-edge XANES of 3d-transition metals. J. Synchrotron Radiat. **6**(3), 315–316 (1999)

Nowotny, J., Sorrell, C.C., Sheppard, L.R., Bak, T.: Solar-hydrogen: environmentally safe fuel for the future. Int. J. Hydrog. Energy **30**(5), 521–544 (2005)

Panella, B., Hirscher, M., Pütter, H., Müller, U.: Hydrogen adsorption in metal-organic frameworks: Cu-MOFs and Zn-MOFs compared. Adv. Funct. Mater. **16**(4), 520–524 (2006)

Ressler, T.: WinXAS: a program for X-ray absorption spectroscopy data analysis under MS-Windows. J. Synchrotron Radiat. **5**(2), 118–122 (1998)

Roland, U., Braunschweig, T., Roessner, F.: On the nature of split-over hydrogen. J. Mol. Catal. A, Chem. **127**(1–3), 61–84 (1997)

Rowsell, J.L.C., Yaghi, O.M.: Metal-organic frameworks: a new class of porous materials. Microporous Mesoporous Mater. **73**(1–2), 3–14 (2004)

Rowsell, J.L.C., Yaghi, O.M.: Effects of functionalization, catenation, and variation of the metal oxide and organic linking units on the low-pressure hydrogen adsorption properties of metal-organic frameworks. J. Am. Chem. Soc. **128**(4), 1304–1315 (2006)

Rowsell, J.L.C., Eckert, J., Yaghi, O.M.: Characterization of H_2 binding sites in prototypical metal-organic frameworks by inelastic neutron scattering. J. Am. Chem. Soc. **127**(42), 14904–14910 (2005)

Saha, D., Deng, S.: Ammonia adsorption and its effects on framework stability of MOF-5 and MOF-177. J. Colloid Interface Sci. **348**(2), 615–620 (2010)

Saha, D., Wei, Z., Deng, S.: Equilibrium, kinetics and enthalpy of hydrogen adsorption in MOF-177. Int. J. Hydrog. Energy **33**(24), 7479–7488 (2008)

Sakintuna, B., Lamari-Darkrim, F., Hirscher, M.: Metal hydride materials for solid hydrogen storage: a review. Int. J. Hydrog. Energy **32**(9), 1121–1140 (2007)

Stuckert, N.R., Wang, L., Yang, R.T.: Characteristics of hydrogen storage by spillover on Pt-doped carbon and catalyst-bridged metal organic framework. Langmuir **26**(14), 11963–11971 (2010)

Suzuki, T., Yamaguchi, T., Hamamoto, K., Fujishiro, Y., Awano, M., Sammes, N.: A functional layer for direct use of hydrocarbon fuel in low temperature solid-oxide fuel cells. Energy Environ. Sci. **4**(3), 940–943 (2011)

Uhm, S., Jeon, H., Kim, T.J., Lee, J.: Clean hydrogen production from methanol-water solutions via power-saved electrolytic reforming process. J. Power Sources **198**, 218–222 (2012)

Wang, L., Stuckert, N.R., Chen, H., Yang, R.T.: Effects of Pt particle size on hydrogen storage on Pt-doped metal-organic framework IRMOF-8. J. Phys. Chem. C **115**(11), 4793–4799 (2011)

Wang, L., Yang, R.T.: Molecular hydrogen and spillover hydrogen storage on high surface area carbon sorbents. Carbon **50**(9), 3134–3140 (2012)

Zabinsky, S.I., Rehr, J.J., Ankudinov, A., Albers, R.C., Eller, M.J.: Multiple-scattering calculations of x-ray-absorption spectra. Phys. Rev. B **52**(4), 2995–3009 (1995)